# *Sky view factor calculations and its application in urban heat island studies*

Urban Climate 30 (2019) 100498

Contents lists available at ScienceDirect

Urban Climate

journal homepage: www.elsevier.com/locate/uclim

# Sky view factor calculations and its application in urban heat island studies

M. Dirksen[a,*], R.J. Ronda[b], N.E. Theeuwes[c], G.A. Pagani[a]

[a] KNMI, Utrechtseweg 297, De Bilt, The Netherlands
[b] Wageningen University & Research, Droevendaalsesteeg 4, Wageningen, The Netherlands
[c] University of Reading, RG6 6AH, United Kingdom

ARTICLE INFO

*Keywords:*
Sky view factor
UHI
Urban planning
Netherlands

ABSTRACT

The sky view factor (*SVF*) is essential to describe the urban climatology at scales below 100*m*. This proxy for net radiation depends on the height of the obstacles in its surroundings. The *SVF* was calculated from a rasterized point cloud height dataset (with $6-10$ points per $m^2$). The resulting *SVF* depends on grid-resolution, search radius and number of directions. Previous research related the diurnal maximum urban heat island (*UHI*) of the canopy layer to the diurnal temperature range, solar irradiance, wind speed, vegetation fraction and *SVF*. The goal of this study is to determine the sensitivity of the *SVF* and the impact on the *UHI*. Within the Netherlands a test area of $70km^2$ was selected, including: urban areas, meadows and forests. There is a high sensitivity for grid-resolution. Therefore the impact of the *SVFs* grid resolution on the maximum *UHI* is explored. Results show that the fourth largest city within the Netherlands, Utrecht, has a mean diurnal maximum *UHI* of 3.1 °C using a 1*m SVF* resolution. But, with a 3*m SVF* resolution the *UHI* is on average 0.6 °C lower. This highlights the significance of a fine grid resolution which can capture houses, alleys and trees.

## 1. Introduction

Since the middle of the 19*th* century global warming equals approximately 1 °C, continuing at this rate it is likely that between 2030 − 2052 we will reach 1.5 °C warming (Masson-Delmotte et al., 2018). Especially heat waves will pose a health risk for large cities. Adaptations within the urban areas are thus required to limit the impact of the urban heat island (*UHI*). Meanwhile the global urbanization continues at a rate of approximately 70 million new inhabitants per year (DESA, 2017). Also the western part of the Netherlands is urbanizing and currently has a population density of over 1000 inhabitants per $km^2$. The Netherlands has a maritime climate with influences from the North Sea. Despite its moderate climate the average daily maximum *UHI* of the urban canopy in Dutch cities is more than 2 °C (Steeneveld et al., 2011). Especially within these densely populated areas, this is expected to lead to thermal discomfort and human health issues (Haines et al., 2006). Studies within several Dutch cities support this concern (Heusinkveld et al., 2014; van der Hoeven & Wandl, 2015; van der Zee & Helmink, 2015). Future scenarios predict higher temperatures during both day and night time (van den Hurk et al., 2006). Without action this is expected to lead to more severe health issues (Haines et al., 2006).

Previous research has shown that there is a clear relationship between the urban morphology on one hand and the local solar irradiance and air temperature on the other hand (Chen et al., 2012; Oke, 1973; Oke, 1982). In order to describe the urban

* Corresponding author.
*E-mail address:* marieke.dirksen@knmi.nl (M. Dirksen).

https://doi.org/10.1016/j.uclim.2019.100498
Received 20 February 2019; Received in revised form 24 May 2019; Accepted 1 July 2019

climatology and its spatial variations the sky view factor (*SVF*) plays a key role (de Morais et al., 2018; Oke, 1973). This fraction of visible sky provides an indication of the street geometry and building density (Gál et al., 2007; Middel et al., 2018; Theeuwes et al., 2017; Zhu et al., 2013). A limited sky view results in increased net heat storage within buildings and an increase of the *UHI*. Trees also limit the *SVF* but do not store much heat, they do limit the outgoing longwave radiation (Klemm et al., 2015; van der Hoeven & Wandl, 2015). Theeuwes et al. (Theeuwes et al., 2017) have shown that for Northwestern European cities the daily maximum UHI ($UHI_{max}$) can be related to the *SVF*, vegetation fraction ($veg_f$) meteorological measurements in the rural area, namely: solar irradiation, diurnal temperature range and wind-speed. The empirical relationship has been verified using citizen weather stations within the city (Bell & Aston University, 2014).

Besides *UHI* studies the *SVF* also has applications in rural areas. As an example river bed morphology studies use the *SVF* to determine vegetation and water characteristics (Bartnik & Moniewski, 2011). Additionally, on a larger scale the *SVF* has applications in down-scaling solar irradiance in complex terrains (Antonanzas-Torres et al., 2014). Numerical studies also considered the *SVF* and $veg_f$ for the prediction of city temperatures. The improved representation of the urban structure showed better simulations of both wind and temperature (de Morais et al., 2018). Several studies on mean radiant temperatures in urban areas used the solar and longwave environmental irradiance geometry (SOLWEIG) model (Lindberg & Grimmond, 2011; Lindberg et al., 2008; Thorsson et al., 2014). The model combines the *SVF* and other city characteristics with meteorological observations (including among others air temperature, relative humidity and solar irradiance) to study heat related mortality. The mean radiant temperature has shown to be a better predictor of heat related mortality than air temperature (Thorsson et al., 2014). For these researches the representation of the urban geometry and vegetation by high resolution *DEMs* is essential (Lindberg & Grimmond, 2011).

The *SVF* can be calculated from different types of data. One can use fish-eye photos (Gál et al., 2007; Middel et al., 2018), but for covering large areas (also off-road) this method is not feasible. Some studies use high resolution 3D building databases (such as Kastendeuch (Kastendeuch, 2013)), for terrain morphology on the other hand, a much coarser digital elevation grid (DEM) is sufficient (Antonanzas-Torres et al., 2014). High resolution DEMs have also been used frequently to calculate the *SVF* (De Wolff, 2008; Gál et al., 2007; Kastendeuch, 2013; Lindberg & Grimmond, 2011). Within the Netherlands there is a point cloud dataset, with 6–10 points per $m^2$ on average, covering the entire country freely available from the Nationaal Georegister (http://nationaalgeoregister.nl). It can be argued that the representation of vertical structures improves using vector based calculations, although on average differences were found to be insignificant with correlations above 98% (Gál et al., 2007). Compared to vector-based *SVF* calculations raster-based calculations are much faster. Considering this and the minimum number of points required for reliable gridding the point cloud will be rasterized on a regular $1m$ grid.

Using the $1m$ DEM the sensitivity for the number of directions, search radius and resolutions will be explored within a test area of $70km^2$ with various terrains (open grass lands, forests and built-up areas). Part of the test area is the city of Utrecht. Utrecht is ranked as fourth largest city of the Netherlands and is located in the central part of the Netherlands. For the city of Utrecht we will calculate the diurnal $UHI_{max}$ of the canopy layer. Our main goal is to determine the *SVF* sensitivity and related $UHI_{max}$. Following the universal semi-empirical $UHI_{max}$ equations presented by (Theeuwes et al., 2017) the impact on the $UHI_{max}$ for the different *SVF* grid resolutions will be established. The computations are performed within the Amazon Web Services (AWS) cloud.

The structure of the paper is as follows. The methodology (Section 2) describes the *SVF* and $UHI_{max}$ equations, datasets required for the *SVF* and $UHI_{max}$ calculations and validation approaches. Next, the results (Section 3) of the *SVF* parameter sensitivity concerning grid resolution, number of directions and radius's are evaluated. This section finishes with the gridded $UHI_{max}$ within the city of Utrecht, followed by the discussion (Section 4) and conclusions (Section 5).

## 2. Methodology

### 2.1. Sky view factor definition

The *SVF* is the fraction of visible sky. The *SVF* is important to determine the surface radiation balance (Theeuwes et al., 2017; Zeng et al., 2018). The short wave radiation within an open terrain (with a *SVF* close to one) reaches the surface without being blocked, while within a more complex terrain (with a *SVF* lower than one) reflections plays a role (Fig. 1a,b). The long wave radiation is either absorbed or reflected by the surface. Part of the long wave radiation is emitted by the surface (Fig. 1c,d). Within urban areas the complex 3D surfaces allows for more opportunities of emission and absorption. The long wave radiation in an open field is reflected in all directions while in the other case the buildings are the limiting factor (Hämmerle et al., 2011; Helbig & Löwe, 2014). Fig. 1f illustrates the *SVF* within a street canyon, due to the building blocks the amount of heat released during daytime is limited (van der Hoeven & Wandl, 2015). From a 2D perspective the *SVF* from a point in the street canyon (Fig. 1f) is estimated as (De Wolff, 2008):

$$SVF_{2D} = \cos\left(\arctan\left[\frac{H}{0.5W}\right]\right) \tag{1}$$

Were $H$ is the height of the obstacle and $W$ is distance between the obstacles. Using Eq. (1) an error estimate of a $1m$ grid used to calculate the 2D central street *SVF* can be derived. Lanes and sidewalks typically have a width of $3m$ and $4m$ respectively. Considering a typical building height of $18m$ and a road with two lanes and sidewalks on both sides the true SVF can be calculated as following: $SVF_{true} = cos\left(arctan\left[\frac{18}{0.5 \cdot 14}\right]\right) = 0.36$. Rasterizing a point cloud will results in deviations around vertical building structures, assuming that the $1m$ on both sides of the road is not represented well in the DEM (i.e. the gridded heights on both sides of the street are not

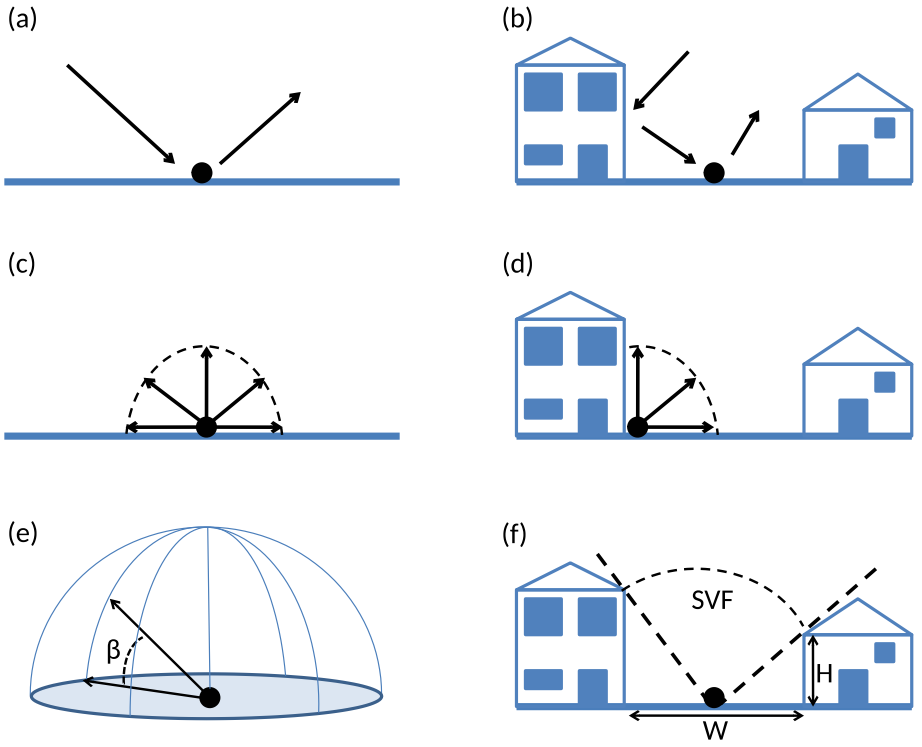


**Fig. 1.** Radiation components in an open field and street canyon and, *SVF* calculations illustrated. (a) Short wave radiation in an open field. (b) Short wave radiation in a street canyon. (c) Emission of long wave radiation in an open field. (d) Emission of long wave radiation in a street canyon. (e) *SVF* calculated in 3D; were, $\beta$ is the angle from the center point to the maximum obstacle height (Eq. (2)). (f) *SVF* in a 2D street canyon; were $W$ is the street width and $H$ is the building height (Eq. (1)). Figures are adapted from (De Wolff, 2008; Hämmerle et al., 2011).

influencing the *SVF* calculations) the estimated SVF from the $1m$ grid equals: $SVF_{estimate} = cos\left(arctan\left[\frac{18}{0.5 \cdot 16}\right]\right) = 0.41$. The maximum SVF underestimation in the central part of a standard street canyon thus equals 12%. Earlier estimates, comparing vector and raster based SVF calculations found correlations on the larger scale of approximately 98% (Gál et al., 2009).

What we refer to as the true SVF in the paper thus is an estimate to the actual SVF with an expected underestimation between 2% and 12%.

From a 3D perspective, according to the parameters in Fig. 1e, the *SVF* for a point on a grid is calculated as:

$$SVF = \int_{\theta=0}^{2\pi} \cos^2(\beta(R,\theta))d\theta \tag{2}$$

Were $\beta$ is the angle from the center point to the maximum obstacle height at a maximum distance equal to the constant search radius ($R$). When integrating this formula over all directions ($d\theta$) from 0 to 2π, the *SVF* for the full hemisphere is obtained.

There are no specific guidelines to determine the minimum grid resolution concerning SVF studies within urban and rural areas. Also different parameter settings for the number of search directions and search radius's have been used to calculate the *SVF* (e.g. (De Wolff, 2008; Dozier & Frew, 1990; Helbig & Löwe, 2014)), though no elaboration on sensitivity of the parameter settings was found. In general calculating the *SVF* using 16 different directions and a search radius of 100 m to detect obstacles limiting the sky view is good enough (Dozier & Frew, 1990). One can imagine that if the number of directions is low not all the obstacles will be detected, the same holds for the search radius. In this study we will perform a sensitivity analysis for these three parameters (grid resolution, search radius and number of directions).

### 2.2. Height dataset

In the Netherlands the height of the landscape has been scanned with LiDAR (Light Detection And Ranging) technology, using airborne laser scanning. By flying overlapping paths during clear weather conditions a high density accurate dataset has been collected. Each path has its own georeference, which is measured on-board. This high resolution DEM model, “Algemeen Hoogtebestand Nederland 2” (AHN2), covers the whole Netherlands. The AHN2 dataset consists of over 40.000 files (Sitek et al., 2006). Each file contains the clouds of points representing the DEM of approximately a $1km$-by-$1km$ area. The overall size of the dataset adds up to more than 1.5 TB in a highly compressed (LAZ) format (Isenburg, 2013). The AHN2 measurements have been collected over the period 2007–2012. The region of Utrecht has been measured in 2008. The AHN2 dataset has a point density

**Table 1**
Overview of the different radii, directions and resolutions used for the sensitivity analysis. All the possible combinations were explored during the *SVF* sensitivity analysis.

| | |
|---|---|
| Resolution (m) | 1, 2, 3, 4, 5, 10, 20, 50 |
| Direction (#) | 2, 3, 4, 8, 16, 32, 64 |
| Radius (m) | 5, 10, 25, 50, 100, 200, 400, 800 |

between 6 and 10 points per $m^2$, making this dataset suitable to capture small scale height differences. The measurements have a systematic error of approximately 3*cm* with a mean standard deviation of 4*cm* (van der Zon, 2013). The measurements exclude water bodies, which are masked during our analysis. The AHN2 has captured buildings, trees and other obstacles for a single moment in time. The height of some of these obstacles may vary through time and new object can emerge or disappear, moreover seasonal changes are not captured.

### 2.3. Sky view factor calculations

The *SVF* is calculated within R (R Development Core Team, 2008) using the *horizon* package (Van Doninck, 2016), similar to Eq. (2) and equations used in (Dozier & Frew, 1990). Calculating the *SVF* from a DEM requires a predefined search radius, number of directions, and grid resolution. The *horizon* package's *SVF* function requires a regularly gridded layer as input. Therefore, the originally irregular points from AHN2 point cloud are projected on a regular grid, using the *raster* package. The work-flow was included in Fig. 3. First, the point cloud dataset was rasterized to a regular grid with a resolution of 1*m* (or another setting from Table 1). Next, a small part of the total area (corresponding to one center tile) was examined. The following procedure was followed in order to calculate the *SVF* for one center tile:

1. Identify the neighboring tiles (eight at most) that have one side or point in common with the region of interest.
2. From the neighboring tiles a buffer surrounding the area of interest was constructed. The buffer width of the frame is equal to the search radius.
3. Merge the buffer and the center tile.
4. Compute the *SVF* on the merged region (Van Doninck, 2016).
5. Crop the merged region to the center tile in order to avoid inaccurate *SVF* results in the framing area.
6. Write the *SVF* for the center to a file.

After the *SVF* calculations for one tile are finished the neighboring tile becomes the center tile and the above described steps are repeated. Following this work-flow enabled the splitting of computing processes over 80 cores, each calculating on a different center tile.

### 2.4. Sky view factor sensitivity analysis

Key to this research was a sensitivity analysis. The sensitivity analysis was performed within a test area of approximately 70$km^2$ with urban areas, grassland and forest (Fig. 2). The northeastern part consists mainly of forest. Agricultural grasslands dominate the northwestern to southeastern band. In the western part, the city center of Utrecht is located with smaller towns/suburbs surrounding it. In order to determine the optimal parameter settings the grid resolution, search radius and number of directions are alternated (Table 1). The resolution varies between 1*m* and 50*m*, the radius between 5*m* and 800*m* and the number of directions between two and 64. As a reference run, i.e. the "true" *SVF*, a 1*m* resolution, 64 directions and 800*m* radius was used. The similarity of the patterns is quantified by the Pearson correlation coefficient, which has a value between $-1$ and 1, where $-1$ indicates the inverse pattern and 1 is an identical pattern. The Pearson correlation coefficient (*PCC*) is defined as:

$$PCC_{xy} = \frac{(x_i - \overline{x})(y_i - \overline{y})}{\sqrt{\sum_{i=1}^{n}(x_i - \overline{x})^2} \cdot \sqrt{\sum_{i=1}^{n}(y_i - \overline{y})^2}} \tag{3}$$

Here, $n$ is the number of grid points, $x_i$, $y_i$ are the grid samples of the tested and representative grid, and $\overline{x}$ is the sample mean (similar for $\overline{y}$) defined as:

$$\overline{x} = \frac{1}{n}\sum_{i=1}^{n}(x_i) \tag{4}$$

In order to determine the correlation between the different resolutions (Table 1) they were re-sampled to a 10 m grid. The absolute difference between the sensitivity runs is quantified with the mean absolute error (*MAE*):

$$MAE = \overline{|x_{1\ldots n} - y_{1\ldots n}|} \tag{5}$$

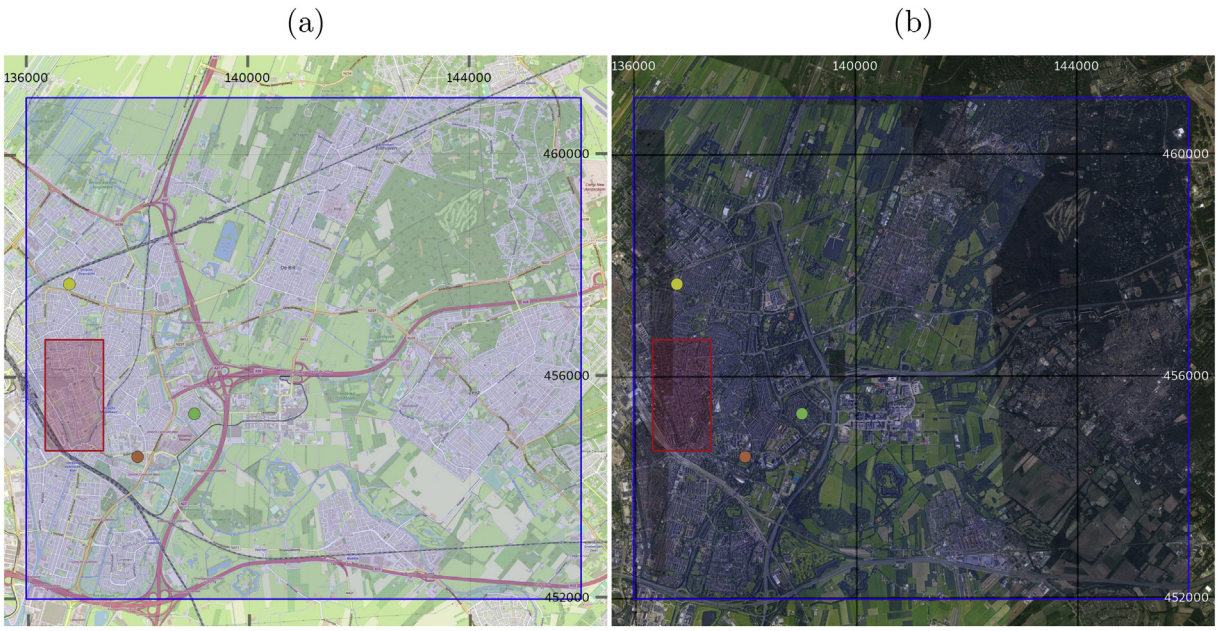


**Fig. 2.** Overview of the sensitivity analysis areas. (a) Terrain map including city names and roads and (b) Satellite image which illustrates the different types of land-use: meadows (light green), forest areas (dark green) and buildings (greyish). Within blue box area the *SVF* sensitivity is explored, the red box was used for the $UHI_{max}$ analysis. The colored dots indicate the locations of the Wunderground stations within the city of Utrecht (western part of the test area). These images were produced using QGIS ©OpenStreetMap and ©Google satellite imagery. Coordinate reference: (epsg : 28992), units are meters. (For interpretation of the references to colour in this figure legend, the reader is referred to the web version of this article.)

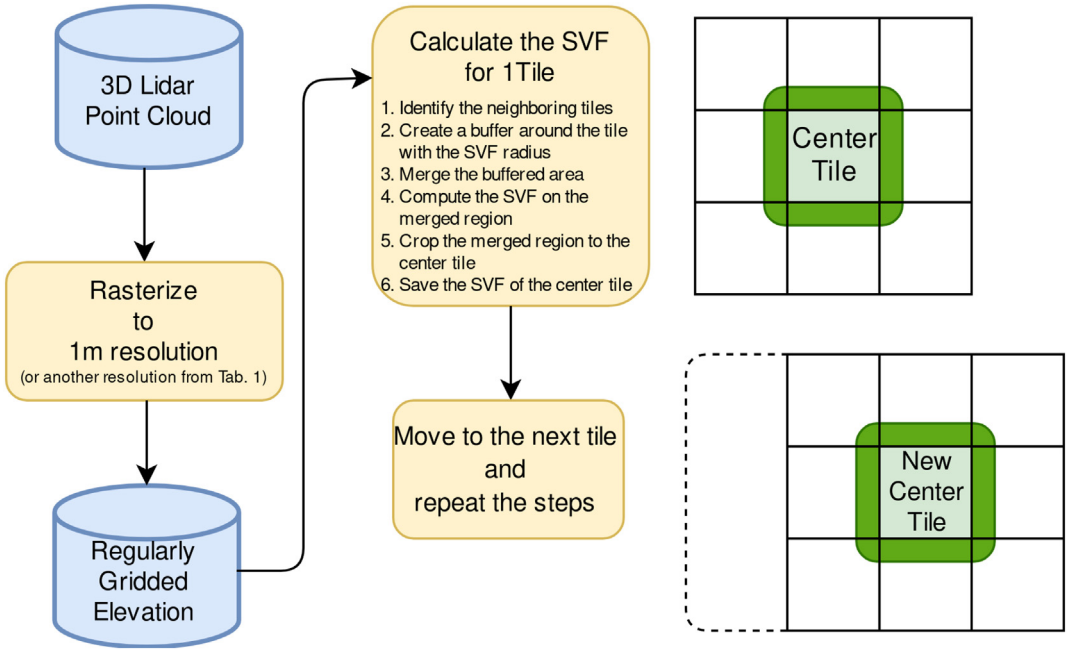


**Fig. 3.** Flow chart of the sky view factor calculations. The point cloud data was regularly gridded on a 1$m$ resolution grid. From the gridded dataset the SVF was calculated for each tile separately. A buffer radius surrounding the tile was added to prevent wrong SVF estimates around the tiles edges. After the results for one tile were saved the SVF for the next tile was calculated.

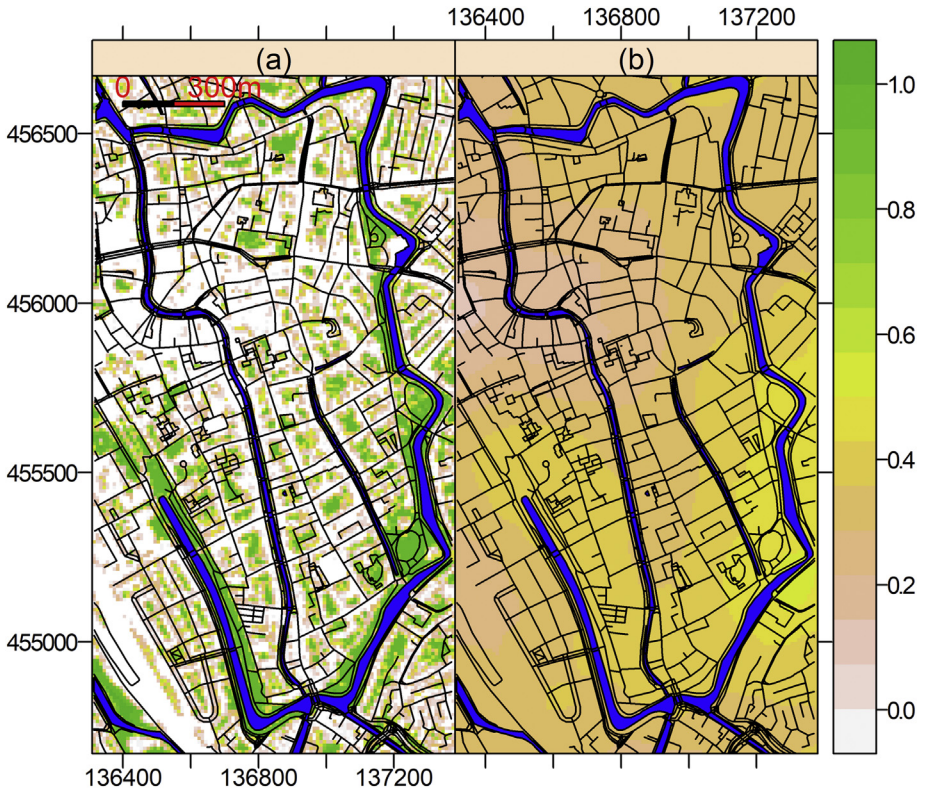


**Fig. 4.** Vegetation fraction in the city center of Utrecht. (a) $veg_f$ without smoothing at a 10$m$ resolution, data source: (Remme et al., 2018). (b) $veg_f$ smoothed with a 250 m radius. The roads are shown as black lines and the water bodies are in blue. The images were produced using ©OpenStreetMap. Coordinate reference: (*epsg* : 28992). (For interpretation of the references to colour in this figure legend, the reader is referred to the web version of this article.)

Here, $x_{1\ldots n}$ and $y_{1\ldots n}$ are the vectors with the values from the tested and representative grid points.

### 2.5. Maximum urban heat island definition

The maximum UHI ($UHI_{max}$) of the urban canopy, derived within Northwest Europe by Theeuwes et al. (Theeuwes et al., 2017), is used by among others Yang et al. (Yang et al., 2019) and Koopmans et al. (Koopmans et al., 2019). The $UHI_{max}$ equation was derived from physical meaningful variables using the key dimension analysis theorem (known as the Buckingham π theorem). Semi-empirically, $UHI_{max}$ is related to the *SVF* as:

$$UHI_{max} = M_{rural} \cdot (2 - SVF - veg_f) \tag{6}$$

Here, $M_{rural}$ are the meteorological variables outside of the city, *SVF* is the *SVF* within the street canyon (since a width/height ratio was used these SVF values relate to street geometry and can thus, in contrast to our estimates, not be related to a certain grid resolution.) and $veg_f$ is the average vegetation fraction within a radius of 500$m$, based on satellite images. Our $veg_f$ and *SVF* definitions slightly differ from Theeuwes et al. (Theeuwes et al., 2017) and are defined in the Sections 2.5.1 and 2.5.2 respectively. $M_{rural}$ depends positively on the solar irradiance (which provides an indication of the energy entering the system) and diurnal temperature range (a higher diurnal temperature range implies more cooling during the night time in the rural area, thus a higher $UHI_{max}$ in the city) and, negatively on the wind speed (a higher wind speed causes additional mixing of air-layer and thus a smaller $UHI_{max}$). The meteorological parameters required from the rural station from Eq. (6) are calculated as:

$$M_{rural} = \sqrt[4]{\frac{DTR^3 \cdot S}{U}} \tag{7}$$

Here, *DTR* is the diurnal temperature range calculated as $T_{max} - T_{min}$, *S* is the mean 24 h solar irradiance and *U* is the daily mean hourly 10 m wind-speed. The equation is only valid if there are no meteorological disturbances such as frontal systems or fog. More detailed information on the equations and valid meteorological conditions can be found in (Theeuwes et al., 2017). Eq. (6) has been evaluated by (Theeuwes et al., 2017) within the ranges:

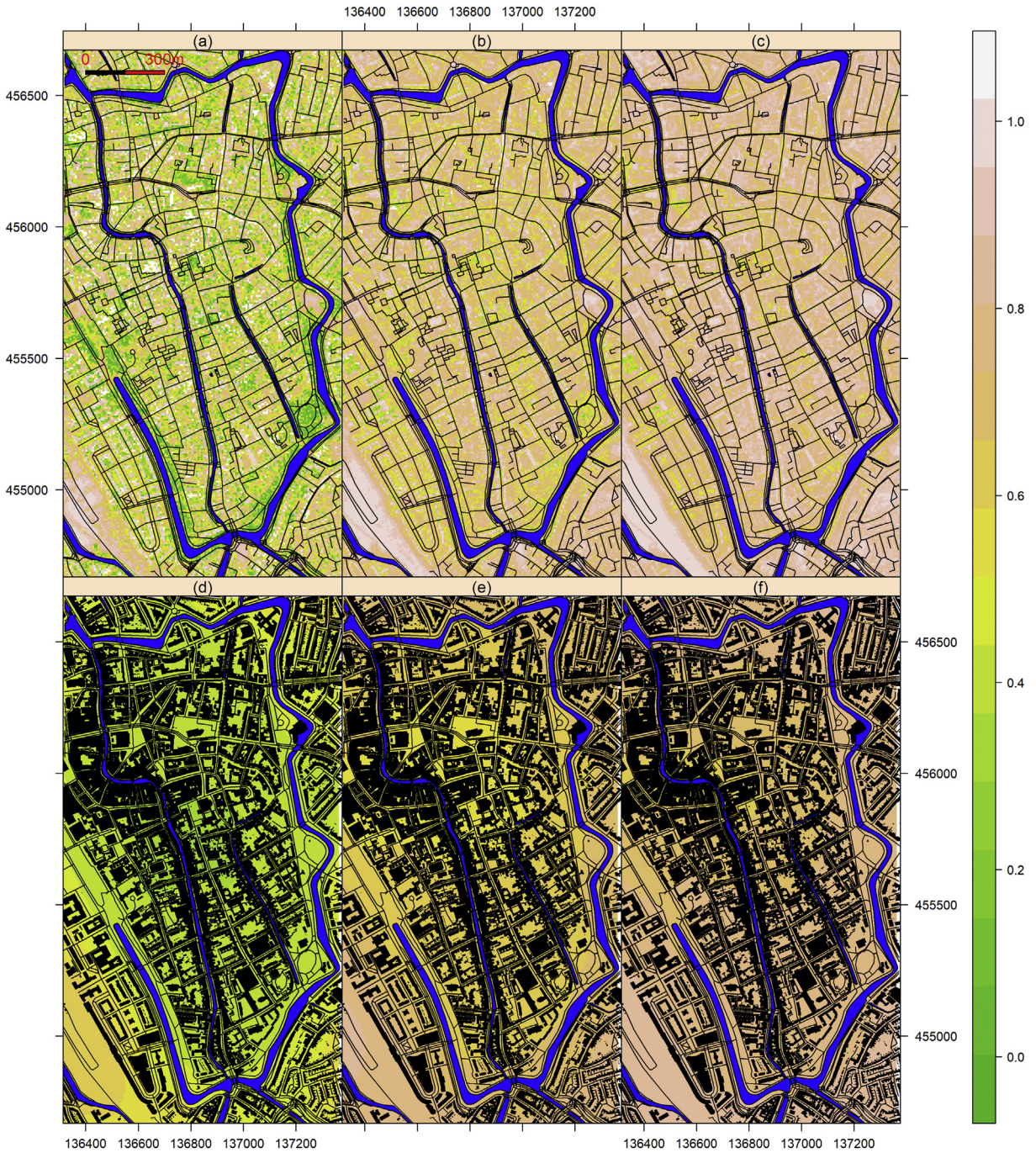


**Fig. 5.** Sky view factor in the city center of Utrecht with different resolutions and smoothing. The top row are the *SVFs* calculated from a (a) 1*m*, (b) 3*m* and (c) 5*m* grid resolution. The bottom row contains the smoothed *SVF* values with a radius of 250*m* and a final resolution of 50*m* derived from (d) the original 1*m* (e) 3*m* and (f) SVF 5*m* grids. The roads are shown as black lines and the water bodies are in blue. The images were produced using ©OpenStreetMap. Coordinate reference: *epsg*: 28992. (For interpretation of the references to colour in this figure legend, the reader is referred to the web version of this article.)

$$0 < veg_f < 0.4$$
$$0.2 < SVF < 0.9$$

To demonstrate the usefulness of our derived *SVF*, we applied the $UHI_{max}$ calculations using different *SVFs* from the sensitivity analysis. The $UHI_{max}$ calculations was applied to the fourth largest city of the Netherlands. The city of Utrecht is located in the central part of the Netherlands. The edges of the city are less suitable for the relationship, therefore a limited area within central part of the

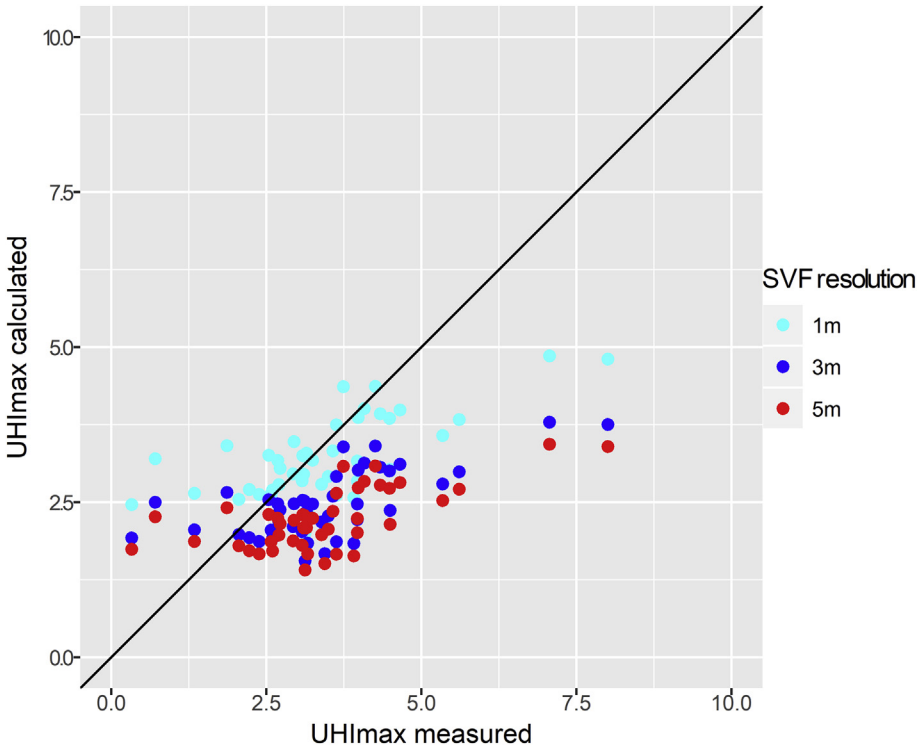


**Fig. 6.** Correlation between the observed $UHI_{max}$ (x-axis) and the semi-empirical relationship (y-axis) from Eq. (6) from (Theeuwes et al., 2017). Colors indicate the different SVF resolutions (cyan, blue and red for respectively the 1*m*, 3*m* and 5*m* resolution) which were smoothed afterwards. (For interpretation of the references to colour in this figure legend, the reader is referred to the web version of this article.)

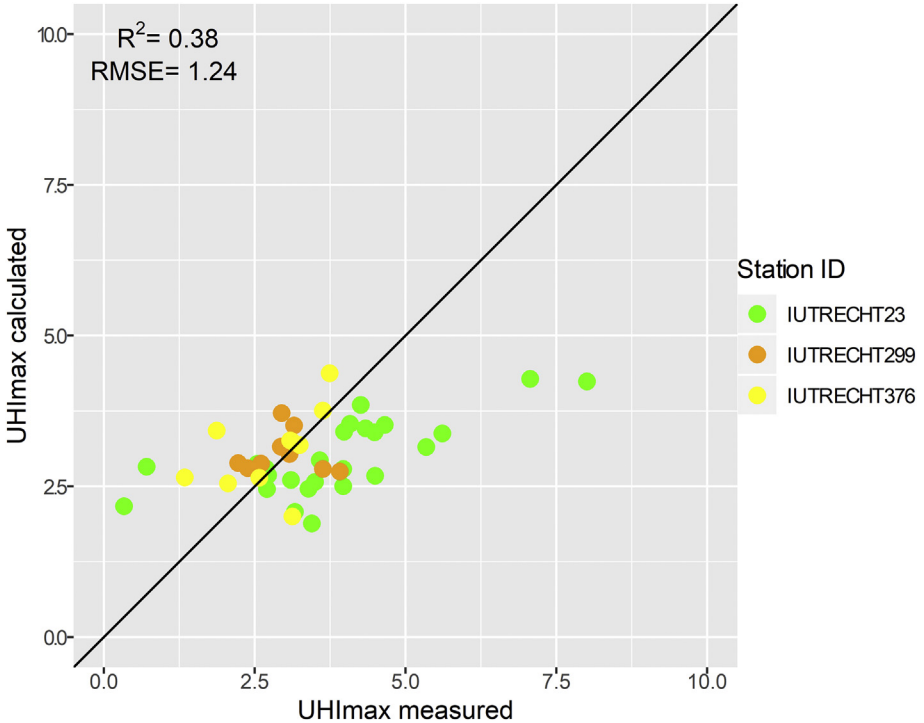


**Fig. 7.** Correlation between the observed $UHI_{max}$ (x-axis) from the rural reference station Cabauw and the Wunderground stations and the empirical relationship (y-axis) from Eq. (6) from (Theeuwes et al., 2017)). Colors of the stations match Fig. 2. The *SVF* was calculated using a radius of 100*m*, 16 directions and a resolution of 1*m* and smoothed afterwards.

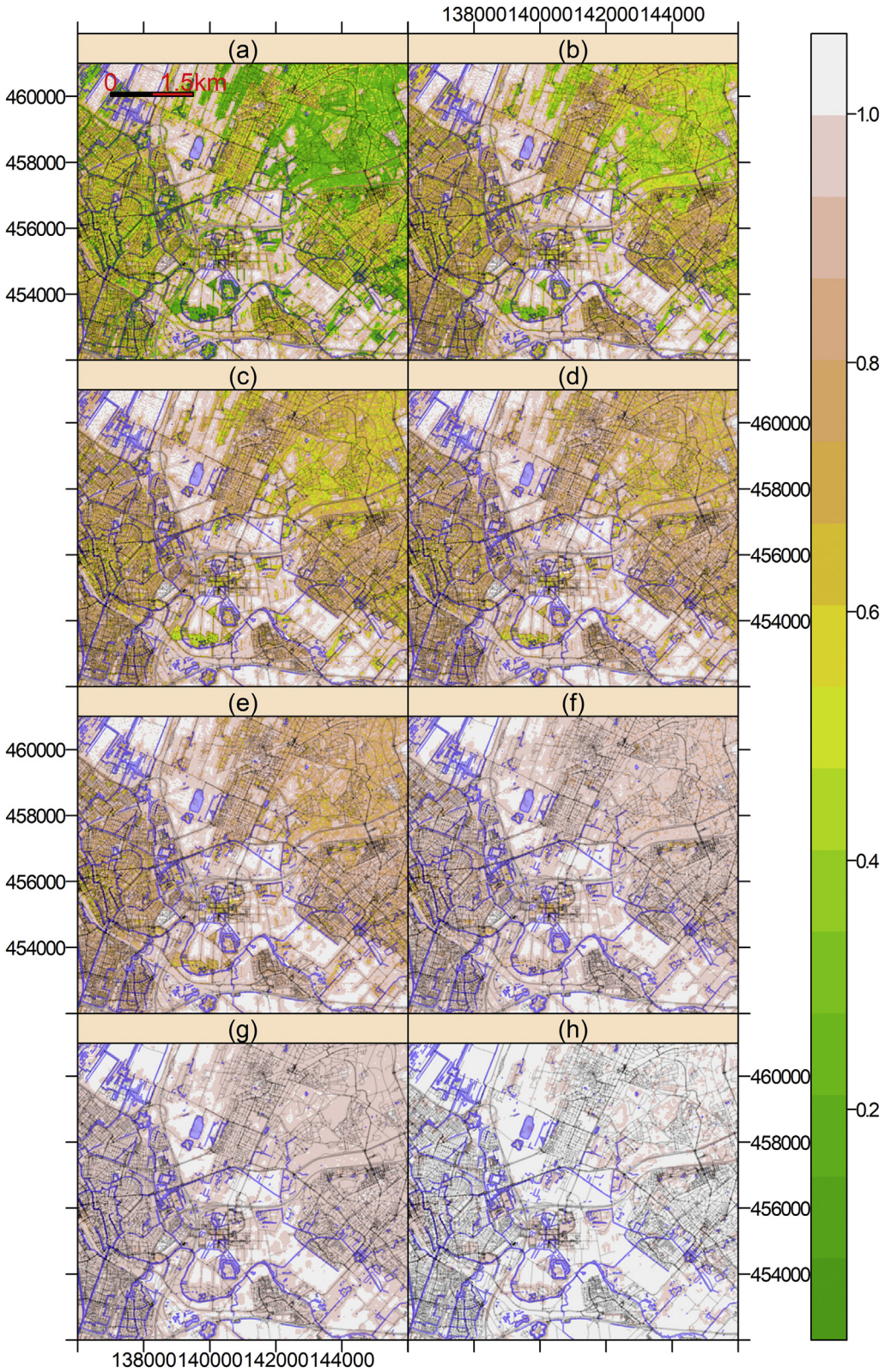


**Fig. 8.** *SVF* sensitivity for different grid resolutions, keeping the directions (16) and radius (100*m*) constant. The resolutions 1*m* (a), 2*m* (b), 3*m* (c), 4*m* (d), 5*m* (e), 10*m* (f), 20*m* (g) and 50*m* (h) are compared. The roads are in grey and waterways are in blue. The images were produced using ©OpenStreetMap. Coordinate reference: (*epsg*: 28992). (For interpretation of the references to colour in this figure legend, the reader is referred to the web version of this article.)

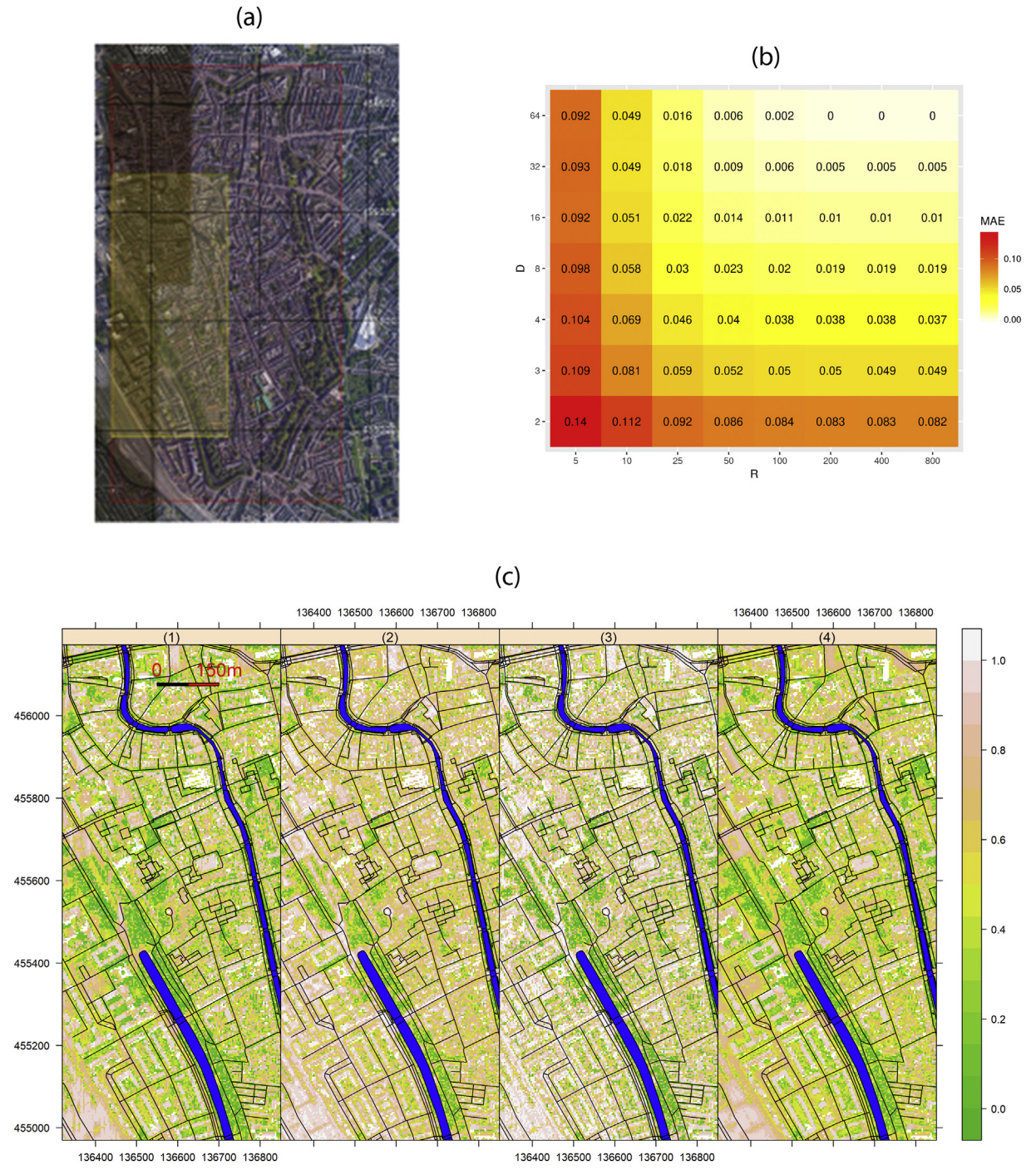


**Fig. 9.** Direction and radius sensitivity of the 1*m SVF*. (a) Satellite image of the city center of Utrecht, in red the $UHI_{max}$ study area. The yellow bounding box is for visually explore differences in *SVF* for R and D. (b) Mean absolute error (Eq. (5)), on the x-axis the different radii (R) and on the y-axis the number of directions (D). The 800 m radius with 64 directions is the reference *SVF*. (c) Zoom of the *SVF* in the city centers yellow box for (1) $D = 2$, $R = 800m$; (2) $D = 64$, $R = 5m$; (3) $D = 2$, $R = 5m$; (4) $R = 64$, $D = 800m$. This image was produced using ©Google satellite imagery. Coordinate reference: (*epsg*: 28992). (For interpretation of the references to colour in this figure legend, the reader is referred to the web version of this article.)

city is selected (see the red bounding box in Fig. 2). Within the city center of Utrecht the smoothed $veg_f$ (Fig.4) and *SVF* (Fig.5) are approximately within the evaluated range. In the following subsections the processing of the different components and application of the equation for this paper are discussed.

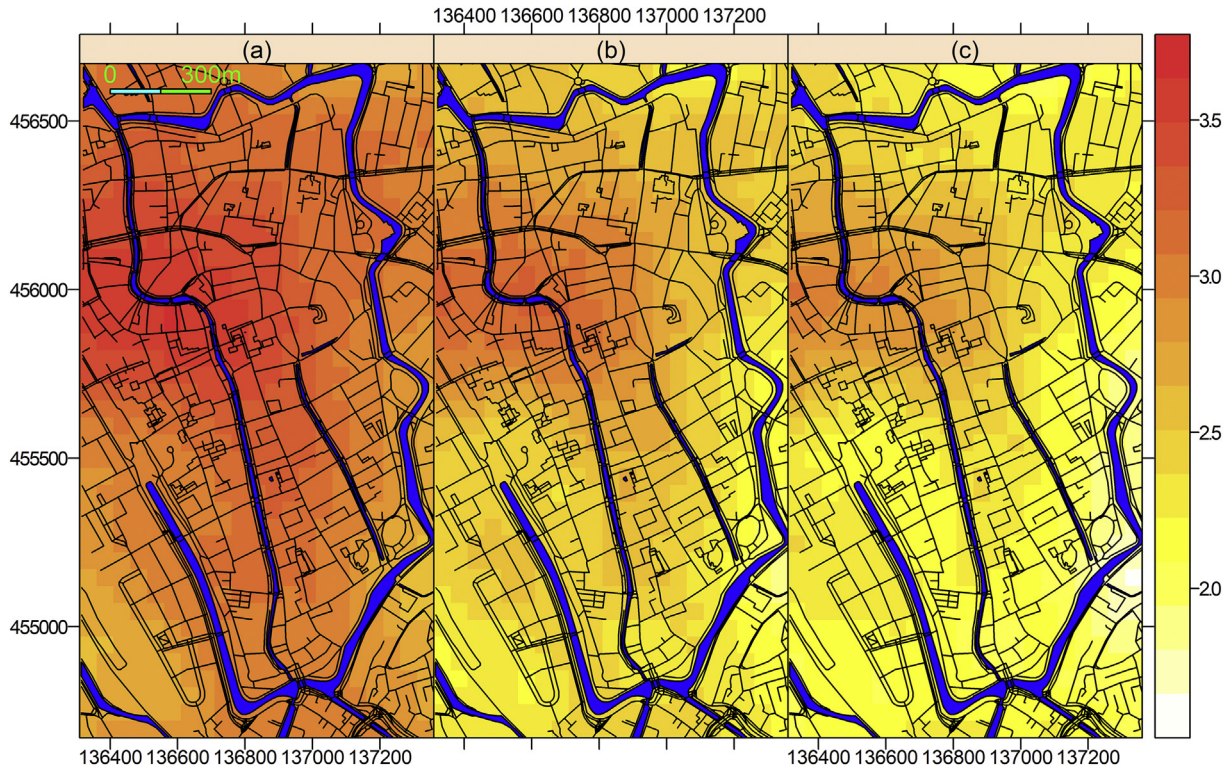


**Fig. 10.** Maximum urban heat island within the streets of the city center of Utrecht. (a) *SVF* with 1*m* resolution, (b) 3*m* and (c) 5*m*. The $UHI_{max}$ varies between 1.6 and 3.3 °C, with a finer *SVF* resolution a stronger $UHI_{max}$ is found. The streets are shown as black lines and in blue the waterways (for interpretability of the spatial patterns buildings are not masked). This image was produced using ©OpenStreetMap. Coordinate reference: (*epsg* : 28992). (For interpretation of the references to colour in this figure legend, the reader is referred to the web version of this article.)

### 2.5.1. Vegetation fraction

For this research we used the 10 m resolution vegetation fraction ($veg_f$) product from (Remme et al., 2018).[1] The $veg_f$ for the Netherlands has been calculated using the AHN2 dataset in combination with other geospatial datasets. Using the high-voltage map, buildings layer database (BAG) and aerial photographs, all from 2016, they masked vegetation and non-vegetation objects. In addition, the Agricultural Areas dataset from the Netherlands (AAN) was used to mask agricultural areas. The height from the remaining vegetation was determined by the difference between the raw AHN2 (including trees and other objects) and the ground-level AHN2. The height of the vegetation was calculated as the difference between the raw AHN2 and ground-level AHN2. Based on the height difference in the $0.5 \cdot 0.5m$ raster file three different vegetation types are distinguished.

- Trees ($> 2.5m$)
- Scrubs ($1.0 - 2.5m$)
- Low vegetation ($< 1.0m$)

The $veg_f$, based on these three different vegetation types, was calculated as follows:

1. All the tree cells were set to a value of 1 and the remaining cells to zero.
2. The $0.5 \cdot 0.5m$ raster files were aggregated to a coarser resolution of $10 \cdot 10m$.
3. The new file contains a tree fraction with a value between zero and one.
4. Step 1 to 3 was repeated for scrubs and low vegetation.

Next, these three layers were summed into one $veg_f$ with values between zero and one.

This methods assumed each vegetation pixel has one type of cover. In order to match the input of formula 6 the $veg_f$ was averaged over an area with a radius of 250 m (Fig. 4). The smoothed $veg_f$ in the northwestern part of the city center is lowest with values around zero. In the northeastern and southeastern part the highest values, up to 0.5, are found. This corresponds with the original $veg_f$ map where most of the vegetation is found in the south and western part of the park surrounding the canal belt.

[1] Available via https://geodata.rivm.nl/downloads/ank/

**Table 2**
Metadata from the wunderground stations in the city center of Utrecht. Each station has a different sensor type. The abbreviation DV for Davis Vantage. The number of observation days with fair weather conditions ranges between 9 − 23 days.

| Station ID | lat,lon | Hardware | *SVF* | *veg* | Years | nr. |
|---|---|---|---|---|---|---|
| IUTRECHT23 | (52.079,5.139) | WS-2902 | 0.58 | 0.49 | 2009–2018 | 23 |
| IUTRECHT299 | (52.086,5.154) | WS-1400-IP | 0.64 | 0.56 | 2018 | 9 |
| IUTRECHT376 | (52.107,5.121) | DV Pro2 | 0.61 | 0.46 | 2016–2018 | 10 |

#### 2.5.2. Sky view factor

Fig. 5 shows the *SVF*, non-smoothed and smoothed, for three different resolutions (1$m$, 3$m$ and 5$m$). In order to obtain a 'street level *SVF*' buildings were removed, using OpenStreetMap, before smoothing within a 250 m radius. The definition of the smoothed *SVF* differs slightly from Theeuwes et al. (Theeuwes et al., 2017) who used the local street canyon *SVF*.

Most of the variations within built-up areas and forests are found between the 1$m$ resolution and the coarser ones. The non-smoothed 1$m$ resolution *SVF* captures smaller alleys and vegetation patches. The representation of these obstacles is limited in the 3$m$ and 5$m$ resolution, resulting in much higher *SVF* values and less spatial variation. Smoothed, the lowest *SVF* values are found within boundaries of the canal belt. The 1$m$ resolution has, averaged over this domain, values around 0.5 while with an increase in resolution to 3$m$ and 5$m$ the mean *SVF* in the center of Utrecht increased to respectively 0.7 and 0.8.

#### 2.5.3. Meteorological rural reference station

The meteorological station Cabauw serves as a reference for the city of Utrecht. The station of Cabauw is within a similar distance (within 20 km) to the city center as other reference stations used in (Theeuwes et al., 2017). The AWS of Cabauw (51.971°$N$,4.927°$E$) is located in a polder landscape around sea level. The solar irradiance was measured with a pyranometer, the temperature with a Pt500 element within a hut and the wind is measured with a cup anemomenter.

#### 2.5.4. Urban meteorological observations

Within the city of Utrecht three citizen weather stations from the Wunderground network (Bell & Aston University, 2014) were used to evaluate Eq. (6): IUTRECHT23 (used by (Theeuwes et al., 2017)), IUTRECHT376 and IUTRECHT299 (Table 2). Theeuwes et al. (Theeuwes et al., 2017) smoothed the $veg_f$ with a radius of 500$m$ and found a lower fraction for IUTRECHT23 of 0.38. As an estimate of the $veg_f$ (Theeuwes et al., 2017) used Google maps. The high resolution $veg_f$ from (Remme et al., 2018) was not available for (Theeuwes et al., 2017). The *SVF* used by (Theeuwes et al., 2017) was estimated using Eq. (1), while our representation is the average over a 250 m radius area (similar to the $veg_f$). Theeuwes et al. (Theeuwes et al., 2017) found a *SVF* of 0.61, compared to our SVF of 0.58 this implies the station is representative for its surroundings. The Wunderground measurements are interpolated in time to match the Cabauw measurements. Considering the application of the $UHI_{max}$ equation and the limited number of observations days, for IUTRECHT23, IUTRECHT299 and IUTRECHT376 respectively 23, 9 and 10, the formula 6 was not adapted for the city of Utrecht. In the next section the correlation between formula 6 and the observations from the city center of Utrecht are compared.

## 3. Results

First, the results from the calculated UHI (from Eq. (6)) were compared with the citizen weather observations. Second, the results of the *SVF* sensitivity analysis for different resolutions, which are based on the blue test area (Fig. 2), are discussed. Third, the number of directions and radii are varied. Although the radius and number of directions can be changed by the user a grid resolution is not something which can be increased. Finally, considering this, the $UHI_{max}$ calculations for the city center of Utrecht, within the red bounding box of Fig. 2, focus on variations in grid resolution.

### 3.1. UHI relationship

In Figs. 6 and 7 the calculated $UHI_{max}$ from Eq. (6), is plotted versus the measured $UHI_{max}$ (calculated as the difference between the rural reference and the different urban stations). From Fig. 6 it can be concluded that the $UHI_{max}$ relationship fits the observed values best for the 1$m$ resolution (while keeping the radius fixed at 100$m$ and the search directions at 16). A high resolution is required to incorporate build up areas. The measured $UHI_{max}$ has a standard deviation of 1.5 °C while the variations of the 1$m$, 3$m$ and 5$m$ are respectively 0.7 °C, 0.6 °C and 0.5 °C. Using a lower resolution results in a â€˜flatteningâ€™ of the SVF and less variation of the UHI. Besides the underestimation of the $UHI_{max}$, a coarser grid resolution thus also loses additional spatial information concerning local temperature variations. A closer examination of the 1$m$ resolution of the different city stations is included in Fig. 7. The 1 : 1 line follows the general trend in the data. Although, during some days the measurements were less representative for the urban area. It is a possibility that some these observations are subject to measurement errors. Two of these possible measurement errors are the observations of IUTRECHT23 with an $UHI_{max}$, measured during mid-day, of 7 °C and 8 °C. During nighttime the $UHI_{max}$ was between 3 and 4. Both days, the 23$th$ and 27$th$ of June 2010, have the highest radiation values (around noon 850$W/m^2$) of the dataset, low wind speeds (approximately 1.5$m/s$) and a DTR of 14. Although the $UHI_{max}$ was measured during the night time, other types of the Ambient Weather Sensor have a radiation-induced bias with these radiation values during the day up to 6.6 °C (Bell & Aston

University, 2014). In contrast, the radiation-induced bias for the Davis Vantage Pro2 series is estimated around 0 °C. The relation coefficient ($R^2$) and root mean square error (*RMSE*) between the observed and measured $UHI_{max}$, within Fig. 7 including the three Wunderground stations, equal 0.38 and 1.24 respectively. Compared to our findings (Theeuwes et al., 2017) found an $R^2$ of 0.65 and an *RMSE* of 0.91. Since it is suspected that the Wunderground measurements of the Ambient Weather Sensor have radiation-induced biases it is expected that the relationship shows some scatter. This is also supported by (Theeuwes et al., 2017), who also found similar scatter. The correlation from fig. 7 is sufficient for the goal of this study. Eq. (6) is representative for the $UHI_{max}$ in Utrecht and the Cabauw measurements can be used as a reference station. As rural meteorological data the median value of the 23 days, between 2009 and 2018, for which IUTRECHT23 measured under relatively calm weather conditions, were used for the $UHI_{max}$ calculations within the city center of Utrecht.

### 3.2. SVF: grid resolution

Fig. 8 presents the *SVF* for different resolutions, while keeping the radius constant at 100*m* and the number of directions at 16. Within the sensitivity area significant height variations are on the scale of buildings, trees and other small obstacles. There are no significant height variations on orography scale. In order to capture the small scale height variations, such as alleys, the resolution of the DEM has to be in the same order of magnitude (one or a few meters). As expected, when the resolution is decreased to 50*m* all the obstacles in the sensitivity area are removed, resulting in a *SVF* of 1. The largest changes from the 1*m* to the 2*m* resolution can be observed in the forests, small towns and city areas. The trees, bushes and alleys need the 1 m resolution to be captured properly. With a further increase to a 5*m* resolution variations between the meadows and the forest and city areas can still be observed. The streets which are wider and have taller buildings can still be distinguished from the 5*m* resolution but disappear almost completely with a 10*m* resolution. Besides this visual comparison also a quantitative comparison was performed. In order to compare the different resolutions quantitatively the results are re-gridded on the 10*m* grid. The Pearson correlation coefficient of the 1*m* resolution compared with the 2*m* and 3*m* equals respectively 0.98 and 0.96. Within the forest and city area the correlation is much lower. With a further decrease in resolution the correlation drops to 0.64 for the 10*m* resolution. In agreement with the visual observations a 10*m* resolution misses all the details already. Combining the visual inspection and correlations a minimum resolution of 3*m* should be used and preferably 2*m* or less. For applications within forests or cities it is recommended to use at least a 1*m* resolution.

### 3.3. SVF: radius and number of directions

Within the yellow bounding box in city center of Utrecht (Fig.9a) the sensitivity for a different number of directions and radii is explored, while keeping the grid resolution fixed at 1*m*. The number of directions in which the *SVF* is calculated are equally distributed in all the directions. The two directions start in a north and south direction. Increasing the number of directions to four also the east and west vectors are covered. A full correlation table for the whole blue bounding box of Fig. 2 is summarized in Fig. 9b. Increasing the number of directions or the radius alone results in a limited improvement of the representation. While, if both the number directions increases and radius is longer the correlation improves significantly. With 16 directions and a 100*m* radius the Pearson correlation coefficient is close to one (0.999), a further increase in the number of directions and radius will not improve the pattern correlation in the test area significantly. The *MAE* of 0.01 is small. Four examples from Fig. 9b are cropped to the yellow bounding box and included in Fig. 9c. The fourth picture of fig. 9c is the 'true' *SVF*, for this case we used 64 search directions and a radius of 800*m*. The first case only uses two directions and a radius of 800*m* and a *MAE* of 0.08. The bottom left corner of this subfigure clearly shows the limits of this approach: only obstacles within this direction can be detected. The second case does search for obstacles in 64 different directions but is limited with a radius of 5*m*, the *MAE* is 0.09. Compared to the previous example and the 'true' *SVF* the values are significantly lower. The third case is limited in both the directions (2) and radius (5 *m*) and results in a higher *SVF*. The *MAE* has increased to 0.14. The same limitations as the 1*m* resolution occur at coarser resolutions. The Pearson correlation coefficient matrix for higher resolutions is slightly worse. For example the 5*m* resolution with 16 directions and a radius of 100*m* has a correlation of 0.997.

### 3.4. Maximum urban heat island

Section 3.2 has shown that major variations in *SVF* can be attributed to variation in grid resolution. Fig. 10 highlights the differences between three different *SVF* resolutions (1*m*, 3*m* and 5*m*). From Eq. (6) we can derive that small decrease in the *SVF* (order 0.1) already has a large impact on the first part of the equation ($2 - SVF - veg_f$) and will result in a higher $UHI_{max}$. Within the city center we find the narrowest streets, while outside of the canal belt the streets are wider. Moreover, the central part also has the lowest vegetation fraction. As so, the city center has the highest $UHI_{max}$ while the regions outside of the canal belt have a lower $UHI_{max}$. Although the pattern of the $UHI_{max}$ is similar, the 1*m* resolution shows the highest $UHI_{max}$ values, which becomes smaller with a lower resolution (Fig. 10). The spatial median $UHI_{max}$ for the 1 m, 3 m and 5 m resolution are respectively: 3.1 °C, 2.5 °C and 2.3 °C. Compared with the 1*m* resolution the 3*m* and 5*m* resolution are on average respectively 0.6 °C and 0.8 °C lower.

## 4. Discussion

The *SVF* sensitivity analysis was performed in a representative area for the Netherlands. Calculating the *SVF* with 16 directions and a search radius of 100 m was, within this terrain type, enough to capture all obstacles and thereby in agreement with (Dozier &

Frew, 1990). This, however, does not imply these settings are applicable for other regions. In hilly and mountainous areas height differences vary on a regional scale.

Whereas the radius and number of directions can be varied, the maximum grid resolution is often predefined by the dataset. With the AHN2 we have been able to analyze at a 1$m$ resolution, but other datasets might not have this level of detail. Especially for applications of the *SVF*, such as the $UHI_{max}$, it is essential that the resolution is equal or preferably smaller than the scale of interest. In our case this implies the *SVF* should capture alleys and other small obstacles. This is supported by Lindberg and Grimmond (Lindberg & Grimmond, 2011).

Eq. (6) from Theeuwes et al. (Theeuwes et al., 2017) was based on 14 different stations across Northwest Europe from which nine were located in the Netherlands (including IUTRECHT23). Taking into account the usage of the $UHI_{max}$ equation by among others Yang et al. (Yang et al., 2019) and Koopmans et al. (Koopmans et al., 2019)), its representativeness for the city center of Utrecht (Fig. 5) and the limited number of observations in the city center of Utrecht we have not adapted Eq. (6) for this specific study. Although the $UHI_{max}$ calculations are accurate within the city center, the interpretation of canal belts park region is questionable with the formula of (Theeuwes et al., 2017)), which has been designed for city centers. With a low *SVF* and a high $veg_f$ Eq. (6) can be simplified to: $UHI_{max} \approx \sqrt[4]{\frac{DTR^3 \cdot S}{U}}$. The *DTR* within forest is lower, with a cooling effect during the day and higher temperatures during night. With the $UHI_{max}$ often occurring during night times this could be a good approximation. We have not been able to verify this due to the lack of measurements within these regions.

According to our calculations the $UHI_{max}$, averaged over 23 selected fair weather conditions according to (Theeuwes et al., 2017), within the city center of Utrecht is above 3 °C for the 1$m$ resolution *SVF*. This is 1 higher than the average UHI of 2 °C suggested by (Steeneveld et al., 2011). For the gridding of $UHI_{max}$ it is important to exclude buildings and only include street level *SVF* values. Omitting this step during the calculations results in a lower $UHI_{max}$ for the 1$m$, 3$m$ and 5$m$ resolutions of respectively 2.8 °C, 2.4 °C and 2.2 °C.

## 5. Conclusions

In this paper we aimed to find the optimal *SVF* parameters settings and the impact of different *SVFs* on the diurnal $UHI_{max}$ of the canopy layer. A sensitivity test was performed on a test area (Fig. 2) of approximately 70$km^2$ and varied the parameters grid resolution, number of directions and search radius (Table 1). Although raster based *SVF* calculations are expected to introduce an underestimation of approximately 2% (Gál et al., 2009) computations are scalable to country level. From the sensitivity analysis it can be concluded that a high resolution incorporates smaller obstacles, resulting in a overall lower *SVF* (Fig. 8) and thus a better approximation of the radiation balance. Within forest and city areas the impact is the largest. The same holds if the number of directions becomes too low. The search radius is sensitive for areas in with alternating height patterns, influencing the sky view, which are varying on a larger scale than the radius itself (Fig. 9). Our recommendation is to use a resolution of 1$m$ or higher. With a number of directions higher than 16 we do not see any significant improvement, therefore we recommend using 16 directions. With a search radius of 100$m$ important obstacles blocking the view are captured, a further increase in search radius does not result in a significant improvement of the *SVF*. Comparing the pattern and bias with a reference run (64 directions and a 800$m$ radius) gives a *PCC* of 0.999 and a *MAE* of 0.01.

Within the city center of Utrecht the *SVF* is significantly lower for the 1$m$ resolution compared to a 3$m$ or 5$m$ resolution. The $UHI_{max}$ equation (Eq. (6)) has been very useful to analyze the impact of differences in *SVF* values on the $UHI_{max}$. As expected the old city center has the highest $UHI_{max}$ while the regions outside of the canal belt have a lower $UHI_{max}$. The average $UHI_{max}$ using the high resolution run within the center is 3.1 °C. Compared with the 1$m$ resolution the 3$m$ and 5$m$ resolution are on average respectively 0.6 °C and 0.8 °C lower. A coarser resolution not only resulted a lower $UHI_{max}$ but temperature variations were found to be smaller and less representative compared to citizen weather temperature observations. Although averaged over an area of 250$m$, the initial resolution of the *SVF* is essential to capture the larger scale empirically founded $UHI_{max}$ relationship (Theeuwes et al., 2017). This level of detail is required to incorporate the alleys of the city center and properly represent the urban morphology.

## Acknowledgment

The authors would like to thank the reviewers for their thoughtful comments and constructive remarks. The authors would also like to thank Ton de Nijs and Harm van Wijnen for their input concerning the vegetation fraction maps. This research has been supported by the Amazon Earth on AWS Cloud Credits for Research program (No. 520409152528). Thanks to this program we have been able to calculate the *SVF* for the entire Netherlands. With our optimized parameter setting this dataset has been made freely available on data.knmi.nl. The code is publicly available on Github (*SVF* and $UHI_{max}$).

## Declaration of interest

Career and intellectual: promotion.

## References

Antonanzas-Torres, F., Martínez-de Pisón, F.J., Antonanzas, J., Perpinan, O., 2014. Downscaling of global solar irradiation in complex areas in R. J. Renew. Sustain.

Ener. 60 (6). https://doi.org/10.1063/1.4901539. 0 063105, nov. ISSN 1941-7012. URL. http://aip.scitation.org/doi/10.1063/1.4901539.
Bartnik, A., Moniewski, P., 2011. River bed shade and its importance in the process of studying of the fundamental Physico-chemical characteristics of Small River waters. Contemp. Probl. Manag. Environ. Prote 70 (0), 137–149 Issues of Landscape Conservation and Water Management in Rural Areas. (doi: 978-83-933953-0-9).
Bell, S., 2014. In: Aston University (Ed.), Quantifying Uncertainty in Citizen Weather Data, PhD thesis. https://ethos.bl.uk/OrderDetails.do?uin=uk.bl.ethos.667723.
Chen, L., Ng, E., An, X., Ren, C., Lee, M., Wang, U., He, Z., 2012. Sky view factor analysis of street canyons and its implications for daytime intra-urban air temperature differentials in high-rise, high-density urban areas of Hong Kong: a GIS-based simulation approach. Int. J. Climatol. 320 (1), 121–136. ISSN 08998418. jan. https://doi.org/10.1002/joc.2243 URL. http://doi.wiley.com/10.1002/joc.2243.
de Morais, M.V.B., de Freitas, E.D., Marciotto, E.R., Guerrero, V.V.U., Martins, L.D., Martins, J.A., 2018. Implementation of observed sky-view factor in a mesoscale model for sensitivity studies of the urban meteorology. Sustainability 100 (7), 2183. 0. ISSN 20711050. jun. https://doi.org/10.3390/su10072183. http://www.mdpi.com/2071-1050/10/7/2183.
De Wolff, R., 2008. Developing an environmental fog potential map using a GIS. In: Technical Report July, KNMI, De Bilt.
DESA, U., 2017. World Population Prospects. United Nations Department of Economic and Social Affairs (UN DESA) Population Division, New York, NY, USA revision edition.
Dozier, J., Frew, J., 1990. Rapid calculation of Terin parameters for radiation Modeling from digital elevation data. IEEE Trans. Geosci. Remote Sens. 280 (5), 963–969. https://doi.org/10.1109/36.58986. 0. ISSN 15580644. http://ieeexplore.ieee.org/document/58986/.
Gál, T., Rzepa, M., Gromek, B., Unger, J., 2007. Comparison between sky view factor values computed by two different methods in an urban environment. ACTA Climatologica Et Chorologica 17–26 Universitatis Szegediensis, Universitatis Szegediensis.
Gál, T., Lindberg, F., Unger, J., 2009. Computing continuous sky view factors using 3D urban raster and vector databases: comparison and application to urban climate. Theor. Appl. Climatol. 950 (1–2), 111–123. 0. ISSN 14344483. jan. https://doi.org/10.1007/s00704-007-0362-9. http://link.springer.com/10.1007/s00704-007-0362-9.
Haines, A., Kovats, R.S., Campbell-Lendrum, D., Corvalan, C., 2006. Climate change and human health: impacts, vulnerability and public health. Public Health 1200 (7), 585–596. 0. ISSN 00333506. jul. https://doi.org/10.1016/j.puhe.2006.01.002. https://www-sciencedirect-com.ezproxy.library.wur.nl/science/article/pii/S0033350606000059?via%3Dihub.
Hämmerle, M., Gál, T., Unger, J., Matzarakis, A., 2011. Introducing a script for calculating the sky view factor used for urban climate investigations. ACTA CLIMATOLOGICA ET CHOROLOGICA 83–92.
Helbig, N., Löwe, H., 2014. Parameterization of the spatially averaged sky view factor in complex topography. J. Geophys. Res.-Atmos. 1190 (8), 4616–4625. https://doi.org/10.1002/2013JD020892. 0. ISSN 21698996.
Heusinkveld, B.G., Steeneveld, G.J., Van Hove, L.W., Jacobs, C.M., Holtslag, A.A., 2014. Spatial variability of the Rotterdam urban heat island as influenced by urban land use. J. Geophys. Res. 1190 (2), 677–692. 0. ISSN 21562202. jan. https://doi.org/10.1002/2012JD019399. http://doi.wiley.com/10.1002/2012JD019399.
Isenburg, M., 2013. Laszip: lossless compression of lidar data. Photogramm. Eng. Remote. Sens. 790 (2), 0 209–217.
Kastendeuch, P.P., 2013. A method to estimate sky view factors from digital elevation models. Int. J. Climatol. 330 (6), 1574–1578. 0. ISSN 08998418. may. https://doi.org/10.1002/joc.3523. http://doi.wiley.com/10.1002/joc.3523.
Klemm, W., Heusinkveld, B.G., Lenzholzer, S., Jacobs, M.H., Van Hove, B., 2015. Psychological and physical impact of urban green spaces on outdoor thermal comfort during summertime in the Netherlands. Build. Environ. 83 (0), 120–128. ISSN 03601323. jan. https://doi.org/10.1016/j.buildenv.2014.05.013. https://www-sciencedirect-com.ezproxy.library.wur.nl/science/article/pii/S0360132314001498.
Koopmans, S., Heusinkveld, B., Steeneveld, G.-j., 2019. Standardization of 1-M Spatial Resolution Urban Heat Maps of Physical Equivalent Temperature to Facilitate Climate Stress Tests in the Netherlands. *EGU abstract*. https://meetingorganizer.copernicus.org/EGU2019/EGU2019-18786-1.pdf.
Lindberg, F., Grimmond, C.S., 2011. The influence of vegetation and building morphology on shadow patterns and mean radiant temperatures in urban areas: model development and evaluation. Theor. Appl. Climatol. 1050 (3), 311–323. 0. ISSN 14344483. oct. https://doi.org/10.1007/s00704-010-0382-8. http://link.springer.com/10.1007/s00704-010-0382-8.
Lindberg, F., Holmer, B., Thorsson, S., 2008. SOLWEIG 1.0 - modelling spatial variations of 3D radiant fluxes and mean radiant temperature in complex urban settings. Int. J. Biometeorol. 520 (7), 697–713. 0. ISSN 00207128. sep. https://doi.org/10.1007/s00484-008-0162-7. http://link.springer.com/10.1007/s00484-008-0162-7.
Masson-Delmotte, V., Zhai, P., Pörtner, H.O., Roberts, D., Skea, J., Shukla, P.R., Pirani, A., Moufouma-Okia, W., Péan, C., Pidcock, R., Connors, S., Matthews, J.B.R., Chen, Y., Zhou, X., Gomis, M.I., Lonnoy, E., Maycock, T., Tignor, M., Waterfield, T., 2018. Global Warming of 1.5 Â°C: An IPCC Special Report on the Impacts of Global Warming of 1.5 Â°C above Pre-Industrial Levels and Related Global Greenhouse Gas Emission Pathways, in the Context of Strengthening the Global Response to the Threat of Climate Chang. IPCC. https://report.ipcc.ch/sr15/pdf/sr15_spm_final.pdf.
Middel, A., Lukaszyk, J., Maciejewski, R., Demuzere, M., Roth, M., 2018. Sky view factor footprints for urban climate modeling. In: Urban Climate. vol. 25. pp. 120–134. ISSN 22120955. sep. https://doi.org/10.1016/j.uclim.2018.05.004 URL. https://www-sciencedirect-com.ezproxy.library.wur.nl/science/article/pii/S2212095518301883.
Oke, T.R., 1973. City size and the urban heat island. In: Atmospheric Environment. vol. 70 (8). pp. 769–779. aug 1973. ISSN 00046981. https://doi.org/10.1016/0004-6981(73)90140-6 URL. https://www.sciencedirect.com/science/article/pii/0004698173901406.
Oke, T.R., 1982. The energetic basis of the urban heat island. Q. J. R. Meteorol. Soc. 1080 (455), 1–24. jan 1982. ISSN 1477870X. https://doi.org/10.1002/qj.49710845502 (URL).
R Development Core Team, 2008. A language and environment for statistical computing. In: R Foundation for Statistical Computing, Vienna, Austria, ISBN 3-900. URL. http://www.r-project.org.
Remme, R., Nijs, T., Paulin, M., 2018. Natural capital model - technical documentation of the quantification, mapping and monetary valuation of urban ecosystem services. In: Technical Report. RIVM, Bilthoven URL. www.rivm.nl/en.
Sitek, A., Huesman, R.H., Gullberg, G.T., 2006. Tomographic reconstruction using an adaptive tetrahedral mesh defined by a point cloud. IEEE Trans. Med. Imaging 250 (9), 1172–1179.
Steeneveld, G.J., Koopmans, S., Heusinkveld, B.G., Van Hove, L.W., Holtslag, A.A., 2011. Quantifying urban heat island effects and human comfort for cities of variable size and urban morphology in the Netherlands. J. Geophys. Res.-Atmos. 1160 (20), D20129. oct 2011. ISSN 01480227. https://doi.org/10.1029/2011JD015988 URL. http://doi.wiley.com/10.1029/2011JD015988.
Theeuwes, N.E., Steeneveld, G.J., Ronda, R.J., Holtslag, A.A., 2017. A diagnostic equation for the daily maximum urban heat island effect for cities in northwestern Europe. Int. J. Climatol. 370 (1), 443–454. jan 2017. ISSN 10970088. https://doi.org/10.1002/joc.4717 URL. http://doi.wiley.com/10.1002/joc.4717.
Thorsson, S., Rocklöv, J., Konarska, J., Lindberg, F., Holmer, B., Konarska, J., Dousset, B., Rayner, D., 2014. Mean radiant temperature a predictor of heat related mortality. Urban Clim. 10, 332–345. dec 2014. ISSN 22120955. https://doi.org/10.1016/j.uclim.2014.01.004 URL. https://www.sciencedirect.com/science/article/pii/S2212095514000054.
van den Hurk, B., Tank, A.K., Lenderink, G., van Ulden, A., van Oldenborgh, G.J., Katsman, C., van den Brink, H., Keller, F., Bessembinder, J., Burgers, G., Komen, G., Hazeleger, W., Driffhout, S., 2006. KNMI climate change scenarios 2006 for the Netherlands. In: Technical Report May. KNMI, De Bilt URL. bibliotheek.knmi.nl/knmipubWR/WR2006-01.pdf.
van der Hoeven, F., Wandl, A., 2015. Amsterwarm: mapping the landuse, health and energy-efficiency implications of the Amsterdam urban heat island. Build. Serv. Eng. Res. Technol. 360 (1), 67–88. https://doi.org/10.1177/0143624414541451. ISSN 0143-6244. URL. http://journals.sagepub.com/doi/10.1177/0143624414541451.
van der Zee, S., Helmink, H., 2015. Luchtverontreiniging Amsterdam. In: Technical Report. GGD Amsterdam, Amsterdam 2017.
van der Zon, N., 2013. Kwaliteitsdocument AHN-2. In: Technical Report. AHN, Amersfoort URL. http://www.ahn.nl/binaries/content/assets/hwh—ahn/common/wat+is+het+ahn/kwaliteitsdocument{_}ahn{_}versie{_}1{_}3.pdf. http://www.ahn.nl/binaries/content/assets/hwh—ahn/common/wat+is+het+ahn/kwaliteitsdocument{_}ahn{_}versie{_}1{_}3.pdf{%}0Ahttp://www.ahn.nl/.

Van Doninck, J., 2016. Package 'horizon'. In: Technical Report. CRAN URL. https://cran.r-project.org/web/packages/horizon/horizon.pdf.

Yang, X., Yao, L., Peng, L.L., Jiang, Z., Jin, T., Zhao, L., 2019. Evaluation of a diagnostic equation for the daily maximum urban heat island intensity and its application to building energy simulations. Ener. Build. 193, 160–173. jun 2019. ISSN 03787788. https://doi.org/10.1016/j.enbuild.2019.04.001 URL. https://www.sciencedirect.com/science/article/pii/S0378778818337290.

Zeng, L., Lu, J., Li, W., Li, Y., 2018. A fast approach for large-scale sky view factor estimation using street view images. Build. Environ. 135, 74–84. may 2018. ISSN 03601323. https://doi.org/10.1016/j.buildenv.2018.03.009 URL. https://www-sciencedirect-com.ezproxy.library.wur.nl/science/article/pii/S0360132318301380.

Zhu, S., Guan, H., Bennett, J., Clay, R., Ewenz, C., Benger, S., Maghrabi, A., Millington, A.C., 2013. Influence of sky temperature distribution on sky view factor and its applications in urban heat island. Int. J. Climatol. 330 (7), 1837–1843. jun 2013. ISSN 1097-0088. https://doi.org/10.1002/JOC.3660 URL. http://doi.wiley.com/10.1002/joc.3660. http://onlinelibrary.wiley.com.ezproxy.library.wur.nl/doi/10.1002/joc.3660/pdf.